ISSN (Print) 1226-1750
ISSN (Online) 2233-6656
Journal of Magnetics 21(1), 40-45 (2016) http://dx.doi.org/10.4283/JMAG.2016.21.1.040

Nickel Substitution Effects on Nano-sized Co, Mn and MnZn Ferrites Synthesized by Sol-gel Method

Won-Ok Choi[1], Woo Hyun Kwon[1], Kwang Pyo Chae[1]*, and Young Bae Lee[2]

[1]*Department of Nano Science and Mechanical Engineering, Nanotechnology Research Center, Konkuk University, Chungju 27478, Korea*
[2]*Department of Physics, Hanzhong University, Donghae 25800, Korea*

(Received 9 December 2015, Received in final form 20 January 2016, Accepted 21 January 2016)

Nickel substituted nano-sized ferrite powders, $Co_{1-x}Ni_xFe_2O_4$, $Mn_{1-x}Ni_xFe_2O_4$ and $Mn_{1-2x}Zn_xNi_xFe_2O_4$ ($0.0 \le x \le 0.2$), were fabricated using a sol-gel method, and their crystallographic and magnetic properties were subsequently compared. The lattice constants decreased as quantity of nickel substitution increased, while the particle size decreased in $Co_{1-x}Ni_xFe_2O_4$ ferrite but increased for the $Mn_{1-x}Ni_xFe_2O_4$ and $Mn_{1-2x}Zn_xNi_xFe_2O_4$ ferrites. For the $Co_{1-x}Ni_xFe_2O_4$ and $Mn_{1-x}Ni_xFe_2O_4$ ($0.0 \le x \le 0.2$) ferrite powders, the Mössbauer spectra could be fitted as the superposition of two Zeeman sextets due to the tetrahedral and octahedral sites of the Fe^{3+} ions. However, the Mössbauer spectrum of $Mn_{0.8}Zn_{0.1}Ni_{0.1}Fe_2O_4$ consisted of two Zeeman sextets and one single quadrupole doublet due to the ferrimagnetic and paramagnetic behavior. The area ratio of the Mössbauer spectra could be used to determine the cation distribution equation, and we also explain the variation in the Mössbauer parameters by using this cation distribution equation, the superexchange interaction and the particle size. The saturation magnetization decreased in the $Co_{1-x}Ni_xFe_2O_4$ and $Mn_{1-2x}Zn_xNi_xFe_2O_4$ ferrites but increased in the $Mn_{1-x}Ni_xFe_2O_4$ ferrite with nickel substitution. The coercivity decreased in the $Co_{1-x}Ni_xFe_2O_4$ and $Mn_{1-2x}Zn_xNi_xFe_2O_4$ ferrites but increased in the $Mn_{1-x}Ni_xFe_2O_4$ ferrite with nickel substitution. These variations could thus be explained by using the site distribution equations, particle sizes and spin magnetic moments of the substituted ions.

Keywords : nickel substituted ferrite, sol-gel method, Mössbauer spectroscopy, saturation magnetization, coercivity

1. Introduction

Ferrites have been used to fabricate components in a wide variety of electromagnetic devises, including microwave and magnetic recorders. Ferrites have a spinel crystal structure (space group Fd3m) in which the O^{2-} ion lattice forms areas with tetrahedral and octahedral local symmetry, which are referred to as A and B sites, respectively. In a normal spinel structure, divalent ions only occupy the A sites, and trivalent ions only occupy the B sites. In an inverse spinel structure, divalent ions occupy half of the B sites, and trivalent ions occupy the rest of the B sites and all A sites. Cobalt ferrite, $CoFe_2O_4$, has cubic spinel structure and has been extensively studied due to its interesting magnetic properties. Cobalt ferrite is basically an inverse spinel for which the corrected cation distribution becomes $(Co_{0.1}Fe_{0.9})[Co_{0.9}Fe_{1.1}]O_4$. The degree of inversion thus depends on the thermal history. Cobalt ferrite has been regarded a competitive candidates for use in high-density magnetic recording media as a result of its high coercivity, moderate saturation magnetization, remarkable chemical stability, and mechanical hardness [1-3]. When manganese ferrite, $MnFe_2O_4$, is prepared at high temperatures (> 1,173 K), 20 % of the Mn^{2+} ions migrate from A to the B sites, and this means that $MnFe_2O_4$ may be characterized as a mixture of normal and inverse spinel ferrite. Manganese ferrite has been widely used in microwave and magnetic recording applications [2]. Mn-Zn ferrites are ceramic materials that are extensively used to fabricate transformers, frequency filters, magnetic recording heads, etc., due to their excellent properties including a high saturation magnetization, high initial permeability, high resistivity and low losses [4]. Nickel ferrite, $NiFe_2O_4$, is a typical soft magnetic material, and its structure has an inverse spinel in which the tetrahedral A sites are occupied by Fe^{3+} ions and the octahedral

*Corresponding author: Tel: +82-43-840-3623
Fax: +82-43-851-4169, e-mail: kpchae@kku.ac.kr

B sites by Fe^{3+} and Ni^{2+} ions [1, 5]. Among ferrospinels, the inverse spinel type is particularly interesting due to its high magnetocrystalline anisotropy and unique magnetic structure. For example, the nickel substituents play an important role in determining the crystallographic and magnetic properties of Co, Mn, and MnZn ferrites, and nickel substitution can also influence the microstructure, intrinsic properties, atomic diffusity and sintering kinetics. One of the advantages of using the sol-gel method is that a lower annealing temperature can be used to enable the growth of smaller grained powders. The sol-gel method can thus provide multi-component oxide with a homogeneous composition, and it has been employed to prepare many high purity oxide powders, including some products with spinel-type structures [6-8].

In this study, the sol-gel method is used to synthesize Ni^{2+} substituted nano-sized Co, Mn and MnZn ferrites, and their crystallographic and magnetic properties were compared by conducting X-ray diffractometry (XRD), scanning electron microscopy (SEM), Mössbauer spectroscopy, and vibrating sample magnetometry (VSM).

2. Experiment

The $CoFe_2O_4$, $Co_{0.8}Ni_{0.2}Fe_2O_4$, $MnFe_2O_4$, $Mn_{0.8}Ni_{0.2}Fe_2O_4$, and $Mn_{0.8}Zn_{0.1}Ni_{0.1}Fe_2O_4$ ferrite samples were synthesized by using the sol-gel method. Measured amounts of Co $(CH_3CO_2)_2{\cdot}4H_2O$, $Ni(NO_3)_2{\cdot}6H_2O$, $Mn(NO_3)_2{\cdot}H_2O$, $Zn(NO_3)_2{\cdot}6H_2O$ and $Fe(NO_3){\cdot}9H_2O$ were first dissolved in 2-Methoxyethanol with an ultrasonic cleaner for 30-50 min. The solution was refluxed at 353 K for 12 h in order to gel, and was dried at 363 K in a dry oven for 24 h. The dried powder samples were ground and annealed at 773 K for 6 h, and all the heat-treatment processes was carried out in an N_2 atmosphere to prevent oxidation of the anion ions. A large amount of N_2 gas flowed early in the annealing process to remove oxygen inside a quartz tube and emitting the gas from a dry powder. In order to verify the purity, all samples were analyzed using an X-ray diffractometer with Cukα (1.54 Å) radiation. The surface microstructure was observed using FESEM at room temperature, and the Mössbauer spectra of the powders were recorded with a ^{57}Co source in a constant acceleration mode to identify the magnetic phase of the ferrite powders. The saturation magnetization and the coercivity were then determined via VSM.

3. Results and Discussion

The X-ray diffraction patterns of the $Co_{1-x}Ni_xFe_2O_4$, $Mn_{1-x}Ni_xFe_2O_4$ and $Mn_{1-2x}Zn_xNi_xFe_2O_4$ ($0.0 \le x \le 0.2$) ferrite powders are shown in Fig. 1. The X-ray diffraction measurement shows that all peaks are consistent with those of typical spinel structures of ferrite powders, and no extra peaks corresponding to any secondary phase were observed. As shown in Table 1, the nickel substitution increases, the lattice constant of the three ferrites decreases for $Co_{1-x}Ni_xFe_2O_4$ from 0.835 nm at x = 0.0 to 0.834 nm at x = 0.2, for $Mn_{1-x}Ni_xFe_2O_4$ decreases from 0.848 nm at x = 0.0 to 0.844 nm at x = 0.2, and for $Mn_{1-2x}Zn_xNi_xFe_2O_4$ also decreases with nickel and zinc substitution from 0.848 nm at x = 0.0 to 0.844 nm at x = 0.1. This can be explained using Vegard's law, which states that the larger Co^{2+} (0.074 nm), Mn^{2+} (0.091 nm) and Zn^{2+} (0.082 nm) ions are substituted by the smaller Ni^{2+} (0.069 nm) ions, leading to a decrease in the lattice constants. The size of the particles was then determined from the diffraction peak broadening with the use of the Scherrer equation [9], $t = (0.9\lambda)/(B\cos\theta_B)$, where λ represent the X-ray wavelength, B is the half width of the (311)

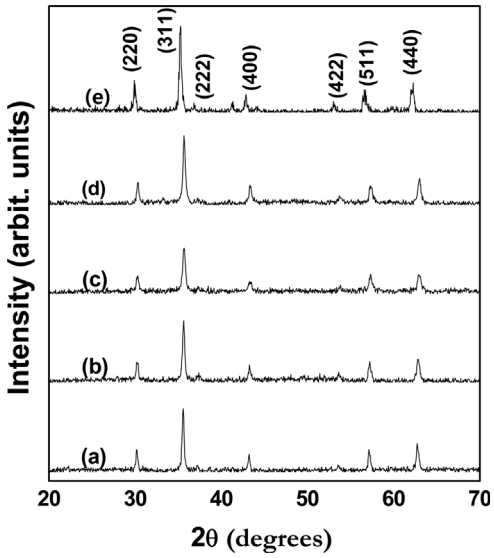

Fig. 1. X-ray diffraction patterns of ferrite powders : (a) $CoFe_2O_4$, (b) $Co_{0.8}Ni_{0.2}Fe_2O_4$, (c) $MnFe_2O_4$, (d) $Mn_{0.8}Ni_{0.2}Fe_2O_4$, and (e) $Mn_{0.8}Zn_{0.1}Ni_{0.1}Fe_2O_4$.

Table 1. Lattice constant and particle size of $Co_{1-x}Ni_xFe_2O_4$, $Mn_{1-x}Ni_xFe_2O_4$ and $Mn_{1-2x}Zn_xNi_xFe_2O_4$ ($0.0 \le x \le 0.2$) ferrite powders.

Sample	Lattice constant (nm)	Particle size (nm)
$CoFe_2O_4$	0.835	25.9
$Co_{0.8}Ni_{0.2}Fe_2O_4$	0.834	25.0
$MnFe_2O_4$	0.848	25.0
$Mn_{0.8}Ni_{0.2}Fe_2O_4$	0.844	26.0
$Mn_{0.8}Zn_{0.1}Ni_{0.1}Fe_2O_4$	0.844	90.0

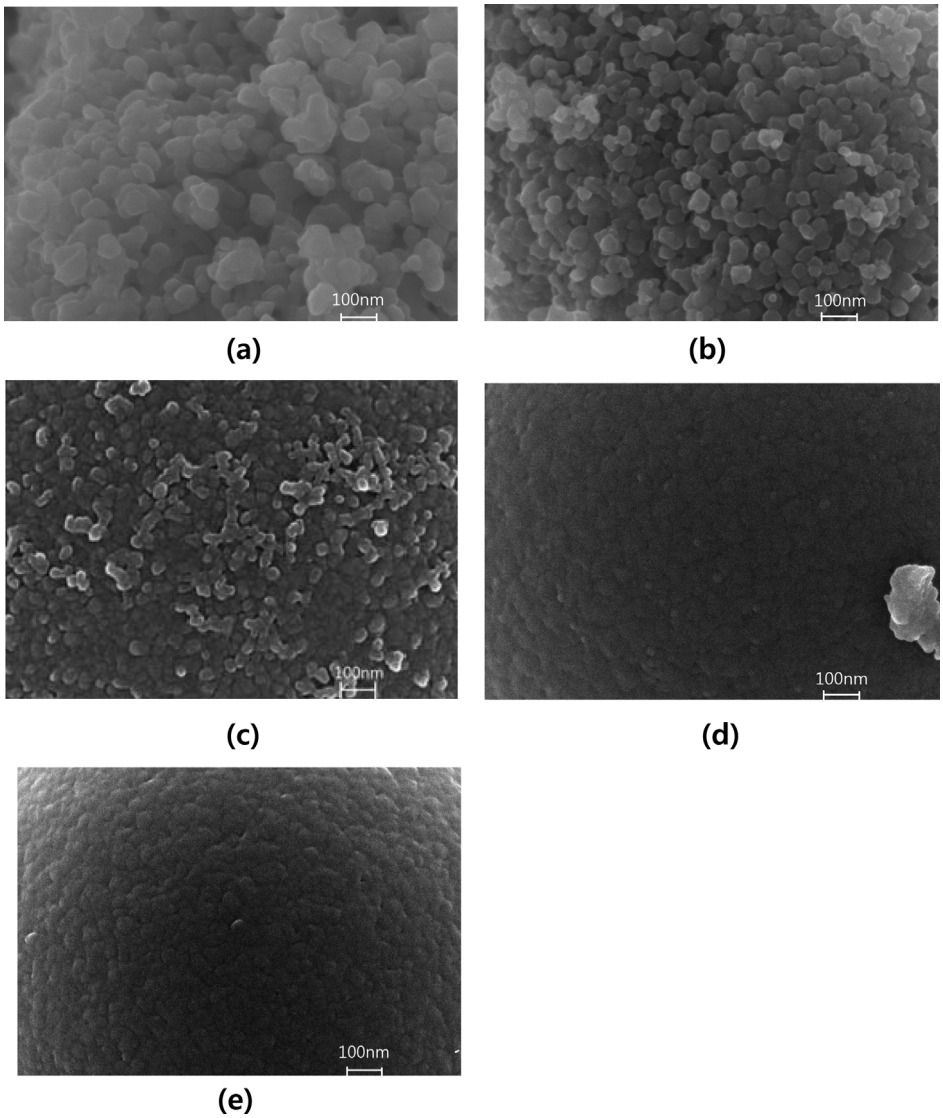

Fig. 2. SEM images (100,000x) of ferrite powders : (a) $CoFe_2O_4$, (b) $Co_{0.8}Ni_{0.2}Fe_2O_4$, (c) $MnFe_2O_4$, (d) $Mn_{0.8}Zn_{0.1}Ni_{0.1}Fe_2O_4$, and (e) $Mn_{0.8}Zn_{0.1}Ni_{0.1}Fe_2O_4$.

peak, and θ_B is the angle of the (311) peak. As shown in Table 1, the particles size for $Co_{1-x}Ni_xFe_2O_4$ decreases with nickel substitution, while those of $Mn_{1-x}Ni_xFe_2O_4$ and $Mn_{1-2x}Zn_xNi_xFe_2O_4$ increase with nickel and zinc substitution. This substitution leads to a broadening of the major peak, that is, a growth of the smaller particle size of our spinel powders as well as to an improved crystallization. The particle size of $Co_{1-x}Ni_xFe_2O_4$ decreases from 25.9 nm at x = 0.0 to 25.0 nm at x = 0.2, but that for $Mn_{1-x}Ni_xFe_2O_4$ increases with nickel substitution from 25.0 nm at x = 0.0 to 26.0 nm at x = 0.2, and that for $Mn_{1-2x}Zn_xNi_xFe_2O_4$ increases 90.0 nm at x = 0.1 with nickel and zinc substitution. All this suggests that the particle size of the nickel substituted cobalt, manganese, and manganese-zinc ferrites powder that were obtained using the sol-gel method are from 25.0 nm to 90.0 nm, which are a smaller size that was comparable to that of powders obtained using ceramic and wet chemical methods. It has been reported that the particle size of $Mn_{1-2x}Zn_xNi_xFe_2O_4$ increased with increasing annealing temperature from 12.2 nm annealed at 473 K to 90.0 nm annealed at 773 K [10]. As shown in Fig. 2, the shape of the grains of the ferrites can be confirmed via FESEM as 100,000 magnifications. All samples have nano-size grains of a nearly homogeneous size, and the grain size decreases as the nickel substitution in $Co_{1-x}Ni_xFe_2O_4$ increases, while those of $Mn_{1-x}Ni_xFe_2O_4$ and $Mn_{1-2x}Zn_xNi_xFe_2O_4$ increase as the nickel and zinc substitution increases.

The Mössbauer absorption spectra that were measured at room temperature for $Co_{1-x}Ni_xFe_2O_4$, $Mn_{1-x}Ni_xFe_2O_4$

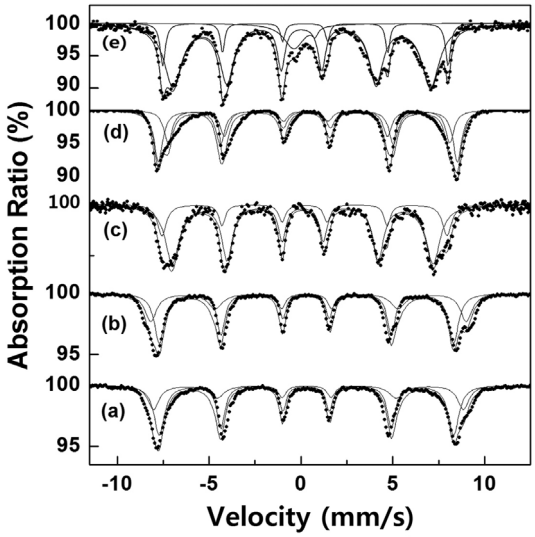

Fig. 3. Mössbauer spectra of ferrite powders at room temperature : (a) $CoFe_2O_4$, (b) $Co_{0.8}Ni_{0.2}Fe_2O_4$, (c) $MnFe_2O_4$, (d) $Mn_{0.8}Ni_{0.2}Fe_2O_4$, and (e) $Mn_{0.8}Zn_{0.1}Ni_{0.1}Fe_2O_4$.

and $Mn_{1-2x}Zn_xNi_xFe_2O_4$ ($0.0 \leq x \leq 0.2$) ferrite powders are shown in Fig. 3 (a)~(d). The spectra of $Co_{1-x}Ni_xFe_2O_4$ and $Mn_{1-x}Ni_xFe_2O_4$ are fitted with two six-line subspectra, and these are assigned to a tetrahedral A site and octahedral B sites of a typical spinel crystal structure. As shown in Table 2, the values of the quadruple splitting (*QS*) and isomer shift (*IS*) of A and B sites are small changed with nickel substitution, while those of the magnetic hyperfine fields (H_{hf}) are increased some in the A and B sites [11, 12, 15]. The increase in the values of the magnetic hyperfine fields indicates that the superexchange interaction is stronger with the nickel substitution in $Co_{1-x}Ni_xFe_2O_4$ and $Mn_{1-x}Ni_xFe_2O_4$, which can be explained by using the cation distribution. The cation distribution depends on many factors, such as the temperature, pressure, and composition [13, 14], as well as the compound preparation method. The Mössbauer absorption area ratio of the A and B sites, and the occupation preference of Ni ions for B sites in a spinel structure, can both be used to determine the cation distribution of $Co_{1-x}Ni_xFe_2O_4$ and $Mn_{1-x}Ni_xFe_2O_4$ as: $(Co_{0.28}Fe_{0.72})[Co_{0.72}Fe_{1.28}]O_4$ for x = 0.0, $(Co_{0.22}Fe_{0.78})$-$[Ni_{0.20}Co_{0.66}Fe_{1.22}]O_4$ for x = 0.2, $(Mn_{0.52}Fe_{0.48})[Mn_{0.48}Fe_{1.52}]O_4$ for x = 0.0, and $(Mn_{0.40}Fe_{0.60})[Mn_{0.40}Ni_{0.2}Fe_{1.40}]O_4$ for x = 0.2. Using this cation distribution equation, we can explain the superexchange interaction being stronger with the nickel substitution. The increase in nickel ions results in a higher magnetic moment for the Fe^{3+} ions (5 u_B) at the A sites, so the A-O-B superexchange becomes stronger in $Co_{1-x}Ni_xFe_2O_4$ and $Mn_{1-x}Ni_xFe_2O_4$ even though the lower magnetic moment Co^{2+} (3 u_B), Fe^{3+} (5 u_B), Mn^{2+} (5 u_B) and Ni^{2+} (2 u_B) ion distribution are somewhat changes. Figure 3 (c) and (e) show the Mössbauer absorption spectra of $Mn_{1-2x}Zn_xNi_xFe_2O_4$ (x = 0.0 and 0.1). The Mössbauer spectrum of the x = 0.0 sample is fitted with two six-line subspectra. However, the spectra of the x = 0.1 sample is fitted with two sextets and one doublet. The area ratio of the doublet decreased some as Zn and Ni substitution increased [15]. The Mössbauer absorption spectra can be explained to be a result of the variation in the magnetic phase resulting due to the particle sizes. As shown for $Mn_{1-2x}Zn_xNi_xFe_2O_4$ ferrite powders [10, 15], the Mössbauer spectra for the x = 0.0 sample annealed at 523 K and the x = 0.1 sample annealed at 473 K are attributed to paramagnetic behavior. This originates from the small particle size, and the superparamagnetic properties were confirmed by the low-temperature Mössbauer spectra. The Mössbauer spectrum for x = 0.1 in the $Mn_{1-2x}Zn_xNi_xFe_2O_4$ ferrite powder is fitted with two six-line subspectra assigned to the A sites and the B sites of the Fe^{3+} ions, as shown in Table 2. The absorption ratio of the Mössbauer Zeeman subspectra and the Mn population data for x = 0.0 in $Mn_{1-2x}Zn_xNi_xFe_2O_4$ can be used to determine the cation distributions as $(Mn_{0.61}Zn_{0.1}Fe_{0.29})[Mn_{0.19}Ni_{0.10}Fe_{1.71}]O_4$ for x = 0.1. This can be compared with $(Zn_xFe_{1-x})[Mn_{1-x}Fe_{1+x}]O_4$ for a Zn-Mn ferrite and $(Mn_{0.52}Fe_{0.48})[Mn_{0.48}Fe_{1.52}]O_4$ for

Table 2. Room temperature Mössbauer parameters of $Co_{1-x}Ni_xFe_2O_4$, $Mn_{1-x}Ni_xFe_2O_4$ and $Mn_{1-2x}Zn_xNi_xFe_2O_4$ ($0.0 \leq x \leq 0.2$) ferrite powders. H_{hf} is the magnetic hyperfine field, *QS* is the quadrupole splitting, and *IS* represent the isomer shift relative to metallic iron at room temperature.

Sample	H_{hf} (kOe)		*QS* (mm/s)		*IS* (mm/s)	
	A site	B site	A site	B site	A site	B site
$CoFe_2O_4$	523.0	497.0	0.05	0.01	0.36	0.29
$Co_{0.8}Ni_{0.2}Fe_2O_4$	532.6	497.5	0.05	0.01	0.36	0.29
$MnFe_2O_4$	481.0	441.1	0.00	0.01	0.30	0.40
$Mn_{0.8}Ni_{0.2}Fe_2O_4$	483.0	445.1	0.01	0.02	0.29	0.41
$Mn_{0.8}Zn_{0.1}Ni_{0.1}Fe_2O_4$	480.9	434.4	0.01	0.06	0.26	0.46
	–	–	1.15		0.31	

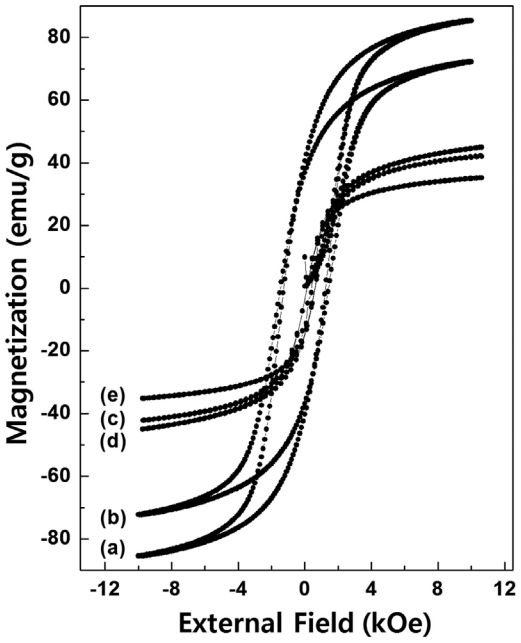

Fig. 4. Hysterisis curves of ferrite powders : (a) $CoFe_2O_4$, (b) $Co_{0.8}Ni_{0.2}Fe_2O_4$, (c) $MnFe_2O_4$, (d) $Mn_{0.8}Ni_{0.2}Fe_2O_4$, and (e) $Mn_{0.8}Zn_{0.1}Ni_{0.1}Fe_2O_4$.

x = 0.0 [16, 17].

The magnetic properties of the $Co_{1-x}Ni_xFe_2O_4$, $Mn_{1-x}Ni_xFe_2O_4$ and $Mn_{1-2x}Zn_xNi_xFe_2O_4$ ($0.0 \leq x \leq 0.2$) ferrite powders can be determined at room temperature by using VSM. Fig. 4 shows the hysteresis curve, and Table 3 shows the changes in the saturation magnetization (M_S) and coercivity (H_C). In the $Co_{1-x}Ni_xFe_2O_4$ ferrite powders, the values of M_s decreased from 85.38 emu/g (x = 0.0) to 72.21 emu/g (x = 0.2) with the nickel substitution. This decrease can be thus be explained by a smaller magnetic moment for Ni^{2+} (2 u_B), as compared to a larger magnetic moment of Co^{2+} (3 u_B). From the cation distribution equation, the Fe^{3+} (5 u_B) distributed between the A and B sites remain almost unchanged, so the M_s values of the $Ni_xCo_{1-x}Fe_2O_4$ ferrites should decrease, by nickel substitution. The H_C values also rapidly decrease from 1,480.0 Oe (x = 0.0) to 1,255.0 Oe (x = 0.2) as the nickel substitution increases. The coercivity in polycrystalline ferrites is well known to strongly depend on the magneto crystalline anisotropy constant, and the grain size. In $Co_{1-x}Ni_xFe_2O_4$ ferrite powders, the grain size does not change abruptly, so the main effect on the coercivity decrease may be a lower magneto crystalline anisotropy constant for Ni^{2+}, with respect to that of Co^{2+}. These results indicate that, the nickel substitute cobalt ferrites show lower coercivity and saturation magnetization, than pure cobalt ferrite powders. In $Mn_{1-x}Ni_xFe_2O_4$ ferrite powders, the values for M_S increased from 42.83 emu/g (x = 0.0) to 45.68 emu/g (x = 0.2) and H_C also increased from 79.2 Oe (x = 0.0) to 119.4 Oe (x = 0.2) with nickel substitution increases, and these changes can be explained by considering the differences in the site distributions and in the spin magnetic moments of the substituted ions. The Mössbauer absorption area showed that the octahedral Mn and Fe ions decreased and the nickel ions increased at x = 0.2. The substitution of ions with greater magnetic moments (Mn^{2+} and Fe^{3+} = 5 u_B) by those with a lesser magnetic moment (Ni $^{2+}$ = 2 u_B) could be expected to reduce the saturation magnetization. However, the results of this work do not support this explanation. Therefore, the nickel ion substitution effects on the saturation magnetization and the coercivity may be concluded to do not be as proportionate to the size of the particle. The XRD and SEM results show that the particles increased in size with nickel ion substitution, and this could have led to an increase in the saturation magnetization and coercivity. Similar reports have been presented for $Co_{0.5}Mn_{0.5}Fe_2O_4$ nanoparticles [18], and in $Mn_{1-2x}Zn_xNi_xFe_2O_4$ ferrite powders the coercivity decreased from 79.2 Oe (x = 0.0) to 64.2 Oe (x = 0.1) as the zinc and nickel substitution increased, and this could be related to the increase in the particle size [14, 15]. The superparamagnetic phase resulting from the smaller particle size changed to a ferrimagnetic phase at x = 0.1, as confirmed by the Mössbauer spectra. The saturation magnetization also some decreased from 42.83 emu/g (x = 0.0) to 36.55 emu/g (x = 0.1) as the zinc and nickel substitution increased. The variation in the saturation magnetization for $Mn_{1-2x}Zn_xNi_xFe_2O_4$ could be qualitatively explained by the superparamagnetic phase due to the particle size and the spin magnetic moment of the substituted ions. The Mössbauer absorption area indicates that the doublet due to the superparamagnetic phase decreased at x = 0.1, and this could produce high values for the saturation magnetization. However, the replacement of ions with a larger magnetic moment ions (Fe^{3+} = 5 u_B) by ions with a smaller magnetic moment (Mn^{2+} = 5 u_B, Ni^{2+} = 3 u_B) could produce low values for the saturation magnetization. As a result of these two effects, the

Table 3. Saturation magnetization (M_s) and coercivity (H_c) of $Co_{1-x}Ni_xFe_2O_4$, $Mn_{1-x}Ni_xFe_2O_4$ and $Mn_{1-2x}Zn_xNi_xFe_2O_4$ ($0.0 \leq x \leq 0.2$) ferrite powders annealed at 773 K.

Sample	M_s (emu/g)	H_c (Oe)
$CoFe_2O_4$	85.38	1,480.0
$Co_{0.8}Ni_{0.2}Fe_2O_4$	72.21	1,255.0
$MnFe_2O_4$	42.83	79.2
$Mn_{0.8}Ni_{0.2}O_4$	45.68	119.4
$Mn_{0.8}Zn_{0.1}Ni_{0.1}Fe_2O_4$	36.55	119.9

saturation magnetization decreases slightly as the Zn and Ni substitution increases [14]. These results reflect a relatively low coercivity and saturation magnetization compared with the values for $MnFe_2O_4$, $Mn_{0.6}Zn_{0.4}Fe_2O_4$, and $Mn_{0.6}Ni_{0.4}Fe_2O_4$ ferrite powders [17, 19].

4. Conclusions

Nickel-substituted nano-sized cobalt, manganese, and manganese-zinc ferrite powders, $Co_{1-x}Ni_xFe_2O_4$, $Mn_{1-x}Ni_xFe_2O_4$ and $Mn_{1-2x}Zn_xNi_xFe_2O_4$ ($0.0 \leq x \leq 0.2$), were fabricated via the sol-gel method, and their crystallographic and magnetic properties were compared. All ferrite powders had a single spinel structure and their lattice constants decreased with the substitution of nickel in $Co_{1-x}Ni_xFe_2O_4$, $Mn_{1-x}Ni_xFe_2O_4$ and $Mn_{1-2x}Zn_xNi_xFe_2O_4$ ferrites, while the particle size decreased in $Co_{1-x}Ni_xFe_2O_4$ ferrite but increased in $Mn_{1-x}Ni_xFe_2O_4$ and $Mn_{1-2x}Zn_xNi_xFe_2O_4$ ferrites.

For the $Co_{1-x}Ni_xFe_2O_4$ and $Mn_{1-x}Ni_xFe_2O_4$ ($0.0 \leq x \leq 0.2$) ferrite powders, the Mössbauer spectra could be fitted as a superposition of two Zeeman sextets due to the tetrahedral and octahedral sites of the Fe^{3+} ions. However, the Mössbauer spectrum of $Mn_{0.8}Zn_{0.1}Ni_{0.1}Fe_2O_4$ consisted of two Zeeman sextets and one single quadrupole doublet as a result of the ferrimagnetic and paramagnetic behavior. The area ratio of the Mössbauer spectra can be used to decide the cation distribution of $Co_{1-x}Ni_xFe_2O_4$ and $Mn_{1-x}Ni_xFe_2O_4$ as: $(Co_{0.28}Fe_{0.72})[Co_{0.72}Fe_{1.28}]O_4$ for x = 0.0, $(Co_{0.22}Fe_{0.78})[Ni_{0.20}Co_{0.66}Fe_{1.22}]O_4$ for x = 0.2, $(Mn_{0.52}Fe_{0.48})[Mn_{0.48}Fe_{1.52}]O_4$ for x = 0.0, $(Mn_{0.61}Zn_{0.1}Fe_{0.29})[Mn_{0.19}Ni_{0.10}Fe_{1.71}]O_4$ for x = 0.1. We also explained the variation of Mössbauer parameters using this cation distribution equation, superexchange interaction and particle size.

The hysteresis curves of the $Co_{1-x}Ni_xFe_2O_4$, $Mn_{1-x}Ni_xFe_2O_4$ and $Mn_{1-2x}Zn_xNi_xFe_2O_4$ ($0.0 \leq x \leq 0.2$) ferrite powders revealed a typical soft ferrite pattern, and the saturation magnetization decreased in the $Co_{1-x}Ni_xFe_2O_4$ ferrite from 85.38 emu/g (x = 0.0) to 72.21 emu/g (x = 0.2) and in the $Mn_{1-2x}Zn_xNi_xFe_2O_4$ ferrite from 42.83 emu/g (x = 0.0) to 36.55 emu/g (x = 0.1), and increased in the $Mn_{1-x}Ni_xFe_2O_4$ from 42.83 emu/g (x = 0.0) to 45.68 emu/g (x = 0.2) with nickel substitution. The coercivity also decreased in the $Co_{1-x}Ni_xFe_2O_4$ from 1,480.0 Oe (x = 0.0) to 1,255.0 Oe (x = 0.2) and in the $Mn_{1-2x}Zn_xNi_xFe_2O_4$ ferrite from 79.2 Oe (x = 0.0) to 64.2 Oe (x = 0.1), and increased in the $Mn_{1-x}Ni_xFe_2O_4$ ferrites from 79.2 Oe (x = 0.0) to 119.4 Oe (x = 0.2) with nickel substitution. These variations could be explained using the site distributions, particle sizes and the spin magnetic moments of the substituted ions.

Acknowledgements

This paper was supported by Konkuk University in 2016.

References

[1] A. Goldman, Modern Ferrite Technology, Van Nostrand Reinhold, New York (1990), p. 217.
[2] N. N. Greenwood and T. C. Gibb, Mössbauer spectroscopy, Chapman and Hall Ltd. London (1971), p. 261-266.
[3] V. Blasko, V. Petkov, V. Rusanov, Ll. M. Martinez, B. Martinez, J. S. Muñoz and M. Mikhove, J. Magn. Magn. Mater. **162**, 331 (1996).
[4] T. Tsutaoka, J. Appl. Phys. **93**, 2789 (2003).
[5] A. S. Albaguergye, J. D. Ardisson and W. A. A. Macedo, J. Appl. Phys. **87**, 4352 (2000).
[6] K. Oda, T. Yoshio, K. Hirata, K. O. Oka and K. Takabashi, J. Jpn. Soc., Powder Powder Metal. **29**, 170 (1982).
[7] V. K. Sankaranarayana, Q. A. Pankhurst, D. P. E. Dickson and C. E. Johson, J. Magn. Magn. Mater. **125**, 199 (1993).
[8] J. G. Lee, J. Y. Park and C. S. Kim, J. Mater. Sci. **53**, 3965 (1998).
[9] B. D. Cullity, Elements of X-Ray Diffraction, Addition Wesley Co. (1978), p. 102.
[10] J. Y. Kang, W. H. Kwon, S. W. Lee, B. S. Kang and K. P. Chae, J. Korean Phys. Soc. **60**, 795 (2012).
[11] P. Didukh, J. M. Grenecheb, A.-S. Waniewska, P. C. Fannin and L. Casas, J. Magn. Magn. Mater. **613**, 242 (2002).
[12] C. V.-Aarca, P. Lavela and J. L. Tirado, J. Power Sources **196**, 6978 (2011).
[13] R. K. Datta and B. Roy, J. Amer. Coram. Soc. **50**, 578 (1967).
[14] M. Z. Schmalzrifd, J. Phys. Chem. **28**, 203 (1961).
[15] W. O. Choi, W. H. Kwon, J. G. Lee, B. S. Kang and K. P. Chae, J. Korean Phys. Soc. **61**, 1812 (2012).
[16] A. S. Albuquerque, J. D. Ardisson and W. A. A. Macedo, J. Appl. Phys. **87**, 4352 (2000).
[17] W. H. Kwon, J. G. Lee, Y. B. Lee and K. P. Chae, J. Magn. **16**, 1 (2011).
[18] M. K. Shobana, S. Sankar and V. Rayendran, Material Chem. Phys. **113**, 10 (2009).
[19] W. H. Kwon, J. Y. Kang, J. G. Lee, S. W. Lee and K. P. Chae, J. Magn. **15**, 159 (2010).